



TRANSIENT RESPONSES IN A FUNCTIONALLY GRADED CYLINDRICAL SHELL TO A POINT LOAD

X. HAN[†] AND D. XU

*Mechanics of Machines Labs, School of Mechanical & Production Engineering,
Nanyang Technological University, 50 Nanyang Avenue, Singapore 639798, Singapore.
E-mail: mxhan@ntu.edu.sg*

AND

G. R. LIU

*Department of Mechanical Engineering, National University of Singapore, 10 Kent Ridge Crescent,
Singapore 119260, Singapore*

(Received 15 November 2000, and in final form 11 June 2001)

A numerical method is proposed for analyzing transient waves in cylindrical shells of a functionally graded material (FGM) excited by impact point loads. In the present method, the FGM shell is divided into layer elements with three nodal lines along the wall thickness. The material property within each element is assumed to vary linearly in the thickness direction, which represents the spatial variation of material property of FGM. This can further reduce the number of elements to obtain more accurate results effectively. The Hamilton principle is used to develop approximate dynamic equilibrium equations. The displacement response is determined by employing the Fourier transformation and the modal analysis. As examples, the displacement responses of FGM shells excited by point loads are calculated, and the characteristics of waves in FGM shells are discussed. The computations have shown the efficiency of the present method.

© 2002 Elsevier Science Ltd.

1. INTRODUCTION

The material properties of structures made of functionally graded material (FGM) vary continuously in the macroscopic sense from one surface to the other. This is achieved by gradually varying the volume fraction of the constituent materials in the manufacturing process. The advantage of FGMs is that they are able to withstand high-temperature-gradient environments while maintaining their structural integrity. In the application of FGM shells to aerospace, nuclear and automobile industries, analyses of transient waves in FGM shells are very important in terms of non-destructive evaluation and material characterization.

There have been considerable works on wave propagation problems related to composite cylindrical shells. Mirsk [1] and Nowinski [2] solved for axially symmetric waves in orthotropic shells respectively. Chou *et al.* [3] provided a three-dimensional (3-D) solution for orthotropic shells as well. Huang and Dong [4] used the finite element method to investigate the wave propagations and the edge vibrations in anisotropic composite

[†]Present address: Centre for ACES, Department of Mechanical Engineering, National University of Singapore, Singapore 119260, Singapore. E-mail: acehanxu@nus.edu.sg

cylinders. Nelson *et al.* [5] proposed a numerical–analytical method (NAM) for analyzing waves in laminated orthotropic cylinders. In the analysis, the circumferential and axial displacements are represented by trigonometric functions, while the radial displacement is modelled by finite elements. Yuan *et al.* [6] proposed an analytical method for the investigation of free harmonic wave propagation in laminated shells, and in their publications, the dispersion behaviors, special cases of infinitely long wavelengths, axisymmetric waves, and degenerate cases of orthotropic shells are described in detail. Nayfeh [7] discussed the scattering of horizontally polarized SH elastic waves from multilayered anisotropic cylinders embedded in isotropic solids. Rattanwangcharoen *et al.* [8] attacked the reflection problem of waves at the free edge of laminated circular shells. Markus and Mead [9, 10] presented an analytical method for investigating the dispersion behavior of waves in orthotropic laminated cylindrical shells. In their treatise, the circumferential and longitudinal displacements are represented by trigonometric functions, whereas the radial displacement is expanded as the Frobenius power series. Xi *et al.* [11] examined waves scattered by a crack in fluid-loaded axisymmetric laminated composite shells. Recently, Han *et al.* [12] investigated the transient responses of axisymmetric FGM cylinders subjected to radial line loads. However, studies on the transient responses of FGM shells subjected to point loads, considered as 3-D problems, have not been found in the literature.

This paper presents an analytical–numerical method to investigate the transient waves in FGM shells subjected to point loads. The FGM shell is divided into a number of cylindrical elements with three nodal lines in the wall thickness. The elemental material properties are assumed to vary linearly in the thickness direction so as to better model the spatial variation of material properties of FGM. The Hamilton’s principle is used to develop the dynamic equilibrium equations. The displacement response is determined by employing the Fourier transform in conjunction with modal analysis. The method is applied to analyze several FGM shells.

2. BASIC EQUATIONS

Consider an FGM shell with varying material properties in the thickness direction. The thickness, inner radius and outer radius of the shell are denoted by H , R_1 , R_2 , respectively, as shown in Figure 1. In view of the heterogeneity of the FGM shell in the radial direction, an annular element shown in Figure 2 is used in the subdivision of the shell so as to achieve high computational precision. The element has inner, middle and outer nodal surfaces I , M , O , and three degrees of freedom (d.o.f.) per nodal surface, u , v , w .

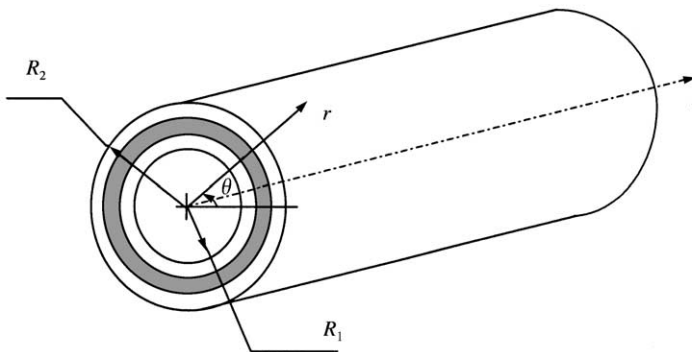


Figure 1. Configuration of an FGM shell.

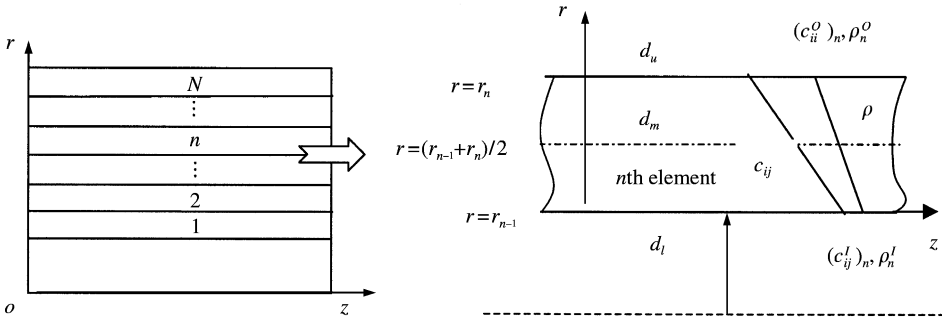


Figure 2. Annular element subdivision and the *n*th isolated annular element.

Suppose that the shell is subdivided into *N* strip elements in the radial direction, and that r_{n-1} and r_n represent, respectively, the inner and outer radii of any element *n*. The elastic coefficient matrix and the mass density on the inner and outer surfaces of the *n*th element are denoted by $\mathbf{c}_n^I = (c_{ij})_n^I (i, j = 1, \dots, 6)$, ρ_n^I , $\mathbf{c}_n^O = (c_{ij})_n^O (i, j = 1, \dots, 6)$ and ρ_n^O , respectively, as shown in Figure 2, where the superscripts “*I*” and “*O*” represent the inner and outer surface respectively. The perfect bonding is assumed. Deformations of the shell are assumed to be small. Under these assumptions, the strain–displacement relations in the cylindrical co-ordinate system are given by

$$\boldsymbol{\varepsilon} = \mathbf{L}\mathbf{U}, \tag{1}$$

where $\boldsymbol{\varepsilon} = [\varepsilon_z \ \varepsilon_\theta \ \varepsilon_r \ \gamma_{r\theta} \ \gamma_{rz} \ \gamma_{z\theta}]^T$ is the vector of strains and $\mathbf{U} = [u \ v \ w]^T$ is the vector of displacements. Here *u*, *v* and *w* are the displacement components in the axial, circumferential and radial directions respectively. The differential operator matrix **L** is given by

$$\mathbf{L} = \begin{bmatrix} \frac{\partial}{\partial z} & 0 & 0 & 0 & \frac{\partial}{\partial r} & \frac{1}{r} \frac{\partial}{\partial \theta} \\ 0 & \frac{1}{r} \frac{\partial}{\partial \theta} & 0 & \frac{\partial}{\partial r} - \frac{1}{r} & 0 & \frac{\partial}{\partial z} \\ 0 & \frac{1}{r} & \frac{\partial}{\partial r} & \frac{1}{r} \frac{\partial}{\partial \theta} & \frac{\partial}{\partial z} & 0 \end{bmatrix} = \mathbf{L}_1 \frac{\partial}{\partial z} + \mathbf{L}_2 \frac{1}{r} \frac{\partial}{\partial \theta} + \mathbf{L}_3 \frac{\partial}{\partial r} + \mathbf{L}_4 \frac{1}{r}, \tag{2}$$

where the matrices **L**₁, **L**₂, **L**₃ and **L**₄ can be obtained by inspecting equation (2).

The stresses are related to strains by

$$\boldsymbol{\sigma} = \mathbf{c}\boldsymbol{\varepsilon}, \tag{3}$$

where $\boldsymbol{\sigma} = [\sigma_z \ \sigma_\theta \ \sigma_r \ \tau_{r\theta} \ \tau_{rz} \ \tau_{z\theta}]^T$ is the vector of stresses and

$$\mathbf{C} = \begin{bmatrix} c_{11} & c_{12} & \cdots & c_{16} \\ & c_{22} & \cdots & c_{26} \\ & & \ddots & \vdots \\ sym & & & c_{66} \end{bmatrix} \tag{4}$$

is the matrix of the off-principal-axis stiffness coefficients of the lamina whose expressions in terms of engineering constants are given by Vinson and Sierakowski [13].

The external traction vector at the inner, middle and outer surfaces of the element are expressed as follows:

$$\mathbf{T}^T = \{\mathbf{T}_I^T \ \mathbf{T}_M^T \ \mathbf{T}_O^T\} \tag{5}$$

in which

$$\mathbf{T}_i^T = \{T_{rz} \ T_{r\theta} \ T_{rr}\}_i \quad (i = I, M, O). \tag{6}$$

The initial conditions of the shell are given by

$$\mathbf{U}|_{t=0} = \mathbf{0}, \ \dot{\mathbf{U}}|_{t=0} = \mathbf{0}. \tag{7}$$

3. ANALYSIS OF TRANSIENT RESPONSES

3.1. DISCRETIZATION IN THE RADIAL DIRECTION

For 3-D problems, the excitation and the field variables of the wave motion are dependent on co-ordinates r, θ, z and t . The equation for the shell method uses annular elements to model the radial displacement component of the shell, while the axial and circumferential displacement components are dealt with analytically.

It is assumed that the material properties of the n th element change linearly in the thickness direction, i.e.,

$$\mathbf{c}_n = (\mathbf{c}_n^O - \mathbf{c}_n^I) \frac{r - r_{n-1}}{r_n - r_{n-1}} + \mathbf{c}_n^I = \Delta \mathbf{c}_{ij}^n \hat{r} + (\mathbf{c}_{ij}^I)_n, \tag{8}$$

$$\rho_n = (\rho_n^O - \rho_n^I) \frac{r - r_{n-1}}{r_n - r_{n-1}} + \rho_n^I = \Delta \rho_n \hat{r} + \rho_n^I. \tag{9}$$

Here $\hat{r} = (r - r_{n-1}) / (r_n - r_{n-1}), r_{n-1} \leq r \leq r_n$. The thickness of the layer element is set as $h_n = r_n - r_{n-1}$.

We approximate the displacement field within the n th element as

$$\mathbf{U} = \mathbf{N}\mathbf{d}, \tag{10}$$

where \mathbf{N} is the shape function matrix of the second order interpolations, and is given by

$$\mathbf{N} = [(1 - 3\hat{r} + 2\hat{r}^2)\mathbf{E} \ 4(\hat{r} - \hat{r}^2)\mathbf{E} \ (2\hat{r}^2 - \hat{r})\mathbf{E}], \tag{11}$$

where \mathbf{E} is a 3×3 identity matrix, and \mathbf{d} contains nodal displacement vectors, and they are functions of the axes z, θ and time t , at $r = r_{n-1}, r = (r_{n-1} + r_n)/2$ and $r = r_n$ as follows:

$$\mathbf{d}^T = \{\mathbf{d}_I^T \ \mathbf{d}_M^T \ \mathbf{d}_O^T\}, \quad \mathbf{d}_i^T = \{d_z \ d_\theta \ d_r\}_i, \quad (i = I, M, O). \tag{12, 13}$$

Application of Hamilton principle yields

$$-\mathbf{B}_1 \frac{\partial^2 \mathbf{d}}{\partial z^2} - \mathbf{B}_2 \frac{\partial^2 \mathbf{d}}{\partial \theta \partial z} - \mathbf{B}_3 \frac{\partial^2 \mathbf{d}}{\partial \theta^2} + \mathbf{B}_4 \frac{\partial \mathbf{d}}{\partial z} + \mathbf{B}_5 \frac{\partial \mathbf{d}}{\partial \theta} + \mathbf{B}_6 \mathbf{d} + \mathbf{M}' \frac{\partial^2 \mathbf{d}}{\partial t^2} = \mathbf{F}, \tag{14}$$

where

$$\mathbf{B}_i = \mathbf{A}_i + \mathbf{A}_i^d \quad (i = 1, \dots, 6), \quad \mathbf{M}' = \mathbf{M} + \mathbf{M}_d, \quad (15, 16)$$

$$\mathbf{F} = \mathbf{T} + \int_0^{h_n} \mathbf{N}^T \mathbf{f} dz. \quad (17)$$

The matrices \mathbf{A}_i ($i = 1, \dots, 6$) and \mathbf{M} are given by

$$\mathbf{A}_1 = \int_{r_{n-1}}^{r_n} \mathbf{N}^T \mathbf{D}_{11} \mathbf{N} r dr, \quad \mathbf{A}_2 = \int_{r_{n-1}}^{r_n} \mathbf{N}^T (\mathbf{D}_{12} + (\mathbf{D}_{12})^T) \mathbf{N} dr, \quad (18, 19)$$

$$\mathbf{A}_3 = \int_{r_{n-1}}^{r_n} \frac{1}{r} \mathbf{N}^T \mathbf{D}_{22} \mathbf{N} dr, \quad (20)$$

$$\mathbf{A}_4 = \int_{r_{n-1}}^{r_n} \left[-\mathbf{N}^T \mathbf{D}_{13} \frac{d\mathbf{N}^T}{dr} + \frac{d\mathbf{N}^T}{dr} (\mathbf{D}_{13})^T \mathbf{N} + \frac{1}{r} \mathbf{N}^T ((\mathbf{D}_{14})^T - \mathbf{D}_{14}) \mathbf{N} \right] r dr, \quad (21)$$

$$\mathbf{A}_5 = \int_{r_{n-1}}^{r_n} \left[-\mathbf{N}^T \mathbf{D}_{23}^I \frac{d\mathbf{N}^T}{dr} + \frac{d\mathbf{N}^T}{dr} (\mathbf{D}_{23}^I)^T \mathbf{N} + \frac{1}{r} \mathbf{N}^T ((\mathbf{D}_{24}^I)^T - \mathbf{D}_{24}^I) \mathbf{N} \right] r dr, \quad (22)$$

$$\mathbf{A}_6 = \int_{r_{n-1}}^{r_n} \left(\frac{d\mathbf{N}^T}{dr} \mathbf{D}_{33} \frac{d\mathbf{N}}{dr} + \frac{1}{r} \frac{d\mathbf{N}^T}{dr} \mathbf{D}_{34} \mathbf{N} + \frac{1}{r} \mathbf{N}^T (\mathbf{D}_{34})^T \frac{d\mathbf{N}}{dr} + \frac{1}{r^2} \mathbf{N}^T \mathbf{D}_{44} \mathbf{N} \right) r dr, \quad (23)$$

$$\mathbf{M} = \int_{r_{n-1}}^{r_n} \mathbf{N}^T \mathbf{N} \rho_n r dr. \quad (24)$$

The detailed expressions for matrices \mathbf{A}_i ($i = 1, \dots, 6$), \mathbf{M} and \mathbf{D}_{11} , \mathbf{D}_{12} , \mathbf{D}_{22} , \mathbf{D}_{13} , \mathbf{D}_{14} , \mathbf{D}_{23} , \mathbf{D}_{33} , \mathbf{D}_{34} are given in Appendix A. \mathbf{f} is the internal body force vector in the element.

The matrices \mathbf{M}_d and \mathbf{A}_i^d ($i = 1, \dots, 6$) are the additional matrices for the variation of the density and the elastic coefficients in the elemental thickness direction, and are given by

$$\mathbf{A}_1^d = \int_{r_{n-1}}^{r_n} \mathbf{N}^T \Delta \mathbf{D}_{11} \mathbf{N} r \hat{r} dr, \quad \mathbf{A}_2^d = \int_{r_{n-1}}^{r_n} \mathbf{N}^T (\Delta \mathbf{D}_{12} + \Delta (\mathbf{D}_{12})^T) \mathbf{N} \hat{r} dr, \quad (25, 26)$$

$$\mathbf{A}_3^d = \int_{r_{n-1}}^{r_n} \frac{1}{r} \mathbf{N}^T \Delta \mathbf{D}_{22} \mathbf{N} \hat{r} dr, \quad (27)$$

$$\mathbf{A}_4^d = \int_{r_{n-1}}^{r_n} \left[-\mathbf{N}^T \Delta \mathbf{D}_{13} \frac{d\mathbf{N}^T}{dr} + \frac{d\mathbf{N}^T}{dr} \Delta (\mathbf{D}_{13})^T \mathbf{N} + \frac{1}{r} \mathbf{N}^T (\Delta (\mathbf{D}_{14})^T - \Delta \mathbf{D}_{14}) \mathbf{N} \right] r \hat{r} dr, \quad (28)$$

$$\mathbf{A}_5^d = \int_{r_{n-1}}^{r_n} \left[-\mathbf{N}^T \Delta \mathbf{D}_{23} \frac{d\mathbf{N}^T}{dr} + \frac{d\mathbf{N}^T}{dr} \Delta (\mathbf{D}_{23})^T \mathbf{N} + \frac{1}{r} \mathbf{N}^T (\Delta (\mathbf{D}_{24})^T - \Delta \mathbf{D}_{24}) \mathbf{N} \right] r \hat{r} dr, \quad (29)$$

$$\mathbf{A}_6^d = \int_{r_{n-1}}^{r_n} \left(\frac{d\mathbf{N}^T}{dr} \Delta \mathbf{D}_{33} \frac{d\mathbf{N}}{dr} + \frac{1}{r} \frac{d\mathbf{N}^T}{dr} \Delta \mathbf{D}_{34} \mathbf{N} + \frac{1}{r} \mathbf{N}^T \Delta (\mathbf{D}_{34})^T \frac{d\mathbf{N}}{dr} + \frac{1}{r^2} \mathbf{N}^T \Delta \mathbf{D}_{44} \mathbf{N} \right) \hat{r} r dr, \tag{30}$$

$$\mathbf{M}^d = \int_{r_{n-1}}^{r_n} \mathbf{N}^T \mathbf{N} \Delta \rho_n \hat{r} r dr. \tag{31}$$

The expressions for matrices \mathbf{A}_i^d ($i = 1, \dots, 6$), \mathbf{M}_d and $\Delta \mathbf{D}_{11}, \Delta \mathbf{D}_{12}, \Delta \mathbf{D}_{22}, \Delta \mathbf{D}_{13}, \Delta \mathbf{D}_{14}, \Delta \mathbf{D}_{23}, \Delta \mathbf{D}_{33}, \Delta \mathbf{D}_{34}$ are given in Appendix B. As it can be seen from equation (14), the original partial differential equations of the shell with four variables (r, θ, z, t) have been simplified into a system of three variables (θ, z, t) using the above procedure.

On assembling the matrices of adjacent elements, we obtain the equation of motion of the whole FGM shell:

$$\mathbf{F}_t = \mathbf{K}_{Dt} \mathbf{d}_t + \mathbf{M}_t \ddot{\mathbf{d}}_t, \tag{32}$$

where

$$\mathbf{K}_{Dt} = -\mathbf{B}_{1t} \frac{\partial^2}{\partial z^2} - \mathbf{B}_{2t} \frac{\partial^2}{\partial \theta \partial z} - \mathbf{B}_{3t} \frac{\partial^2}{\partial \theta^2} + \mathbf{B}_{4t} \frac{\partial}{\partial z} + \mathbf{B}_{5t} \frac{\partial}{\partial \theta} + \mathbf{B}_{6t}. \tag{33}$$

In these equations, the subscript “t” indicates that the matrices correspond to the whole FGM shell, and the matrices $\mathbf{d}_t, \mathbf{M}_t, \mathbf{B}_{it}$ ($i = 1, \dots, 6$) are the results of assembling the contribution of $\mathbf{d}, \mathbf{M}, \mathbf{B}_i$ ($i = 1, \dots, 6$) for neighboring elements respectively. The vectors \mathbf{d}_t and \mathbf{F}_t represent the nodal displacements and the external traction applied at the nodes of the shell respectively. The sizes of \mathbf{d}_t and \mathbf{F}_t , are $M \times 1$ and the sizes of the matrices $\mathbf{K}_{Dt}, \mathbf{M}_t, \mathbf{B}_{it}$ ($i = 1, \dots, 6$) are $M \times M$. If the shell is divided into N elements, $M = 3(2N + 1)$.

3.2. EQUATION IN THE TRANSFORM DOMAIN

The Fourier transformations with respect to the co-ordinates z and θ are introduced as follows:

$$\tilde{\mathbf{d}}_t(k_\theta, k_z, t) = \int_{-\infty}^{+\infty} \int_{-\infty}^{+\infty} \mathbf{d}_t(\theta, z, t) e^{-ik_\theta \theta} e^{-ik_z z} d\theta dz, \tag{34}$$

where $i = \sqrt{-1}$ and the real transformation parameters k_θ and k_z are the wave numbers in the circumferential direction and in the z -axis direction respectively.

The application of the Fourier transform indicated by equations (34) to (32), leads to approximate equations of motion of the FGM shell as follows:

$$\tilde{\mathbf{F}}_t = \mathbf{M}_t \ddot{\tilde{\mathbf{d}}}_t + \mathbf{K}_t \tilde{\mathbf{d}}_t, \tag{35}$$

where $\tilde{\mathbf{F}}_t, \ddot{\tilde{\mathbf{d}}}_t,$ and $\tilde{\mathbf{d}}_t$ are the Fourier transformations of $\mathbf{F}_t, \ddot{\mathbf{d}}_t,$ and \mathbf{d}_t respectively. Matrix \mathbf{K}_t is given as

$$\mathbf{K}_t = k_z^2 \mathbf{B}_{1t} + k_z k_\theta \mathbf{B}_{2t} + k_\theta^2 \mathbf{B}_{3t} - ik_z \mathbf{B}_{4t} - ik_\theta \mathbf{B}_{5t} + \mathbf{B}_{6t}. \tag{36}$$

3.3. DISPLACEMENT VECTOR IN THE FOURIER TRANSFORMATION DOMAIN

The modal analysis [14] is used to obtain the Fourier transformation of the displacement vector. Solving the following eigenvalue equation corresponding to equation (35):

$$\mathbf{0} = [\mathbf{K}_t - \omega^2 \mathbf{M}_t] \boldsymbol{\psi}^R, \tag{37}$$

we can obtain the eigenfrequencies ω_m ($m = 1, 2, \dots, M$) and the corresponding right eigenvectors $\boldsymbol{\psi}_m^R$.

For example, consider the time-step impact load, which can be expressed as

$$\mathbf{F}_t = \mathbf{F}_{0t} \mathbf{H}(t), \tag{38}$$

where $\mathbf{H}(t)$ is the Heaviside time-step function, \mathbf{F}_{0t} is the constant amplitude vector of the applied force. On applying the Fourier transform to equation (38), we get

$$\tilde{\mathbf{F}}_t = \tilde{\mathbf{F}}_{0t} \mathbf{H}(t). \tag{39}$$

By applying the method of modal analysis, and using the initial condition equation (7), the displacement in the Fourier transform domain can be obtained as follows:

$$\tilde{\mathbf{d}}_t(k_z, k_\theta, t) = \sum_{m=1}^M \frac{\boldsymbol{\psi}_m^L \tilde{\mathbf{F}}_{0t} \boldsymbol{\psi}_m^R (1 - \cos \omega_m t)}{\omega_m^2 M_m}, \tag{40}$$

where ω_m , φ_m^R and φ_m^L are the m th eigenfrequency and the corresponding right and left eigenvector. M_m is the equivalent mass of the m th mode and is expressed by

$$M_m = \boldsymbol{\psi}_m^L \mathbf{M}_t \boldsymbol{\psi}_m^R. \tag{41}$$

The time history of the incident wave pressure to the shell is a function of t as

$$\mathbf{F}_t = \begin{cases} \mathbf{F}_{0t} \sin(2\pi t/t_d), & 0 < t < t_d, \\ \mathbf{0}, & t \leq 0 \text{ and } t \geq t_d, \end{cases} \tag{42}$$

where t_d is the time duration of the incident wave and $\omega_f = 2\pi/t_d$.

Using the Duhamel integral and equation (40), we can obtain the displacement in the Fourier transformation domain subjected to the load given by equation (42):

$$\tilde{\mathbf{d}}_t = \begin{cases} \sum_{m=1}^M \frac{\boldsymbol{\psi}_m^L \tilde{\mathbf{F}}_{0t} \boldsymbol{\psi}_m^R (\omega_f \sin(\omega_m t) - \omega_m \sin(\omega_f t))}{(\omega_m^2 - \omega_f^2) M_m \omega_m}, & 0 < t \leq t_d, \\ \sum_{m=1}^M \frac{\boldsymbol{\psi}_m^L \tilde{\mathbf{F}}_{0t} \boldsymbol{\psi}_m^R \{(\omega_f - \omega_m) \sin[(\omega_f + \omega_m)\tau - \omega_m t] - (\omega_f + \omega_m) \sin[(\omega_f - \omega_m)\tau + \omega_m t]\}_j^t}{\boldsymbol{\psi}_m^L M_m \boldsymbol{\psi}_m^R (\omega_f^2 - \omega_m^2) \omega_m}, & t > t_d. \end{cases} \tag{43}$$

3.4. DISPLACEMENT RESPONSES IN THE SPACE-TIME DOMAIN

Taking the inverse Fourier transformation, the displacement response in the space-time domain can be described by

$$\mathbf{d}_t(\theta, z, t) = \frac{1}{4\pi^2} \int_{-\infty}^{+\infty} \int_{-\infty}^{+\infty} \tilde{\mathbf{d}}_t(k_\theta, k_z, t) e^{ik_\theta\theta} e^{ik_z z} dk_\theta dk_z. \quad (44)$$

The integration in equation (44) can be carried out by using the two-dimensional fast Fourier transform (FFT) technique [15].

It should be noted that the angular co-ordinate θ has the limiting domain between $-\pi$ and $+\pi$. Based on the study done by Pierce and Kil [16] that waves propagating in a point-excited thin-walled circular shell behave like waves propagating in a two-dimensional unbounded homogeneous anisotropic medium with excitation forces that are periodic in the circumferential co-ordinates, the displacement response of the shell can be expressed as a superposition of unbounded medium responses.

4. COMPUTATION PROCEDURE

The FGM shell is divided into N layer elements in the thickness direction. If the values of Young's module, the shear module, the Poisson ratio on the inner, middle and outer surfaces of the elements can be calculated from the known functions of thickness, then the elastic coefficient matrices on the lower, middle and upper surfaces of the element can be obtained. The matrices \mathbf{M}_i , \mathbf{B}_i ($i = 1, 2, \dots, 6$) and \mathbf{F} can be established from equations (15–31). Matrices \mathbf{M}_i , \mathbf{B}_{it} and \mathbf{F}_t can be obtained by assembling the matrices \mathbf{M}_i , \mathbf{A}_i ($i = 1, 2, \dots, 6$) of neighborhood elements. For the step-impact force, the frequencies and the corresponding left and right eigenvectors can be calculated by solving equation (37). Using equation (40), the displacement vector in the frequency domain can be obtained. The displacement in the frequency domain for arbitrary loading can be calculated by using the Duhamel integral. Finally, the displacement response can be obtained by using equation (44), where FFT is employed to calculate the integral.

5. NUMERICAL RESULTS

To verify the formulation and implement the present analysis, we calculate an SiC-C FGM, circular cylindrical shell of $\bar{R} = 100$ at the outset. The displacement response on the surface to a sine function line load on the upper surface is depicted in Figure 3, and compared with those obtained by Liu *et al.* [17] for the corresponding SiC-C FGM plate. Because the non-dimensional radius is large, the results of the shell should approach those of the corresponding plate. As expected, a good agreement is observed between them.

Four types of FGM shells composed of stainless steel and silicon nitride are studied. They are all composed of stainless steel and silicon nitride. Types 1 and 2 FGM shells are single-layer shells. The former has stainless steel on its outer surface and silicon nitride on its inner surface while the latter has silicon nitride on its outer surface and stainless steel on its inner surface. Types 3 and 4 FGM shells have two layers. Type 3 has silicon nitride on its outer and inner surfaces and stainless steel on its middle surface. Type 4 has stainless steel on its outer and inner surfaces and silicon nitride on its middle surface. The material properties for stainless steel and silicon nitride are listed in Table 1 [18].

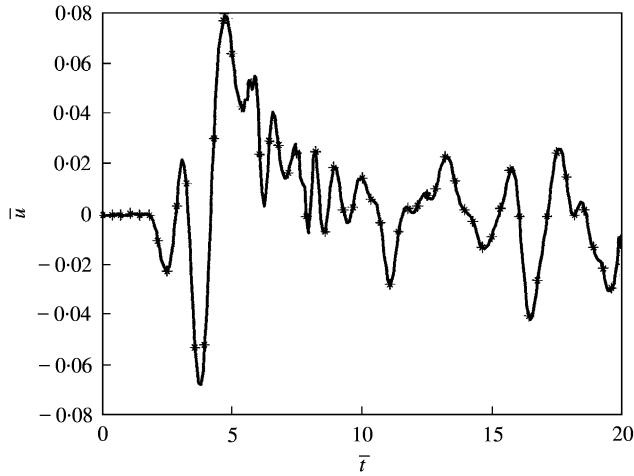


Figure 3. The time history of the displacement at $z = 5H$ on the upper surface on the SiC-C FGM plate excited by an incident wave of one cycle of sine functions at $z = 0$: —, present method; —*, Liu *et al.* (1999).

TABLE 1

Material properties of stainless steel and silicon nitride FGM [18]

Coefficients	Stainless steel			Silicon nitride		
	$E(\text{GPa})$	ν	$\rho (\text{kg/m}^3)$	$E(\text{GPa})$	ν	$\rho (\text{kg/m}^3)$
P_0	201.04	0.3262	8166	348.43	0.24	2370
P_{-1}	0	0	0	0	0	0
P_1	3.079×10^{-13}	-2.002×10^{-4}	0	-3.07×10^{-13}	0	0
P_2	-6.534×10^{-16}	3.97×10^{-7}	0	2.160×10^{-16}	0	0
P_3	0	0	0	-68.946×10^{-20}	0	0
	207.82	0.3177	8166	322.4	0.24	2370

For Types 1 and 2 FGM shells, the volume fraction can be expressed as

$$V_{m1}(\hat{r}) = (\hat{r})^n, \quad V_{m2}(\hat{r}) = 1 - (\hat{r})^n, \quad \hat{r} \in [0, 1], \tag{45}$$

where n is the power-law exponent. The value of n is determined by optimization for minimum uniform stress across the thickness. For Type 1 FGM shell, V_{m1} represents the volume fraction of stainless steel and V_{m2} represents the volume fraction of silicon nitride. For Type 2 FGM shell, V_{m1} stands for the volume fraction of silicon nitride and V_{m2} the volume fraction of stainless steel. Thus, the variation of volume fraction for Type 2 shell with radial position z in the thickness direction is in contrast with that of Type 1 FGM shell.

For Types 3 and 4 FGM shells with two layers, the volume fraction can be expressed as

$$V_{m1}^1(\hat{r}) = (\hat{r})^n, \quad V_{m2}^1(\hat{r}) = 1 - (\hat{r})^n, \quad \hat{r} \in [0, 0.5], \tag{46}$$

$$V_{m1}^2(\hat{r}) = (2\hat{r} - 1.0)^n, \quad V_{m2}^2(\hat{r}) = 1 - (2\hat{r} - 1.0)^n, \quad \hat{r} \in [0.5, 1]. \tag{47}$$

For Type 3 FGM shell, V_{m1}^k ($k = 1, 2$) represents the volume fraction of stainless steel and V_{m2}^k ($k = 1, 2$) represents the volume fraction of silicon nitride. For Type 4 FGM shells, V_{m1}^k ($k = 1, 2$) represents the volume fraction of stainless steel and V_{m2}^k ($k = 1, 2$) represents the volume fraction of silicon nitride. Therefore, the variations of V_{m1}^k , V_{m2}^k ($k = 1, 2$) with radial position in the thickness direction are opposite to that for Type 3 FGM shell.

The incident wave pressure to the shell is assumed to be a load acting on the upper surface of the shell. \mathbf{F}_{or} is a constant vector

$$\mathbf{F}_{or} = \{0, 0, \dots, q_0\}, \quad (48)$$

where q_0 is the amplitude of the load.

Since the present method is based on the three-dimensional elasticity theory, it is applicable to both a circular cylindrical shell and circular shell with any ratio of thickness to radius. In order to explore the distinction between waves in both, two ratios of radius to thickness $R_1/H = 1, 20$ are used in the present calculations. The shell with $R_1/H = 1$ is viewed as a thick shell, while the latter is viewed as a cylindrical shell.

5.1. DISPLACEMENT RESPONSES EXCITED BY POINT LOADS

The point impact load \mathbf{F}_t is assumed as

$$\mathbf{F}_t = \mathbf{F}_{or} f(t) \delta(z) \delta(\theta), \quad (49)$$

where $f(t)$ is the function of time, $\delta(z)$ and $\delta(\theta)$ are the Dirac delta functions of z and θ respectively. Equation (49) describes vertical point loads acting on the upper surface of a shell. In this subsection, only the responses of the displacement in r and z directions on the upper surface of the shell are considered, and the following dimensionless parameters are used:

$$\begin{aligned} \bar{u} &= u/u_0, & u_0 &= Hq_0/G_0, & \bar{t} &= t/t_0, & t_0 &= H/c_0, & c_0 &= \sqrt{G_0/\rho_0}, \\ \bar{w} &= w/u_0, & \bar{\omega} &= \omega H/c_0, & \bar{x} &= x/H, & \bar{z} &= z/H, & \bar{r} &= r/H, & \bar{\rho} &= \rho/\rho_0, \end{aligned} \quad (50)$$

where ρ_0 , G_0 , c_0 and t_0 are the mass density, the shear modulus, the velocity of shear wave for a referenced material and the time for shear wave of referenced material to cross the shell thickness once. The material property on the inner surface of the shell under consideration is taken as the referenced material property. In this paper, we set $\bar{t}_d = 2.0$. It means that the incident wave is a wavelet of one cycle of the sine function.

Figures 4–7 illustrate the response distributions of the radial displacement w on the upper surface for these four-type thick shells. In these calculations, the value of the power-law exponent n is set to 1.0, and the radial point load at ($z = 0$, $\theta = 0$) with a time history of one cycle sine function. From these four figures, we can see as to how the displacement response distributes on the outer surface of the FGM shells. Type 4 FGM shell has better property for attenuation of the displacement response induced by the same stress source of excitation, as the peak value of displacement response of Type 4 shell is the smallest.

Figure 8 shows the time history of the displacement \bar{u} on the outer surface of the Type 1 cylindrical shell subjected to a point load at point ($z = 0$, $\theta = 0$) on the outer surface. A comparison of the displacement responses between various values of the power-law

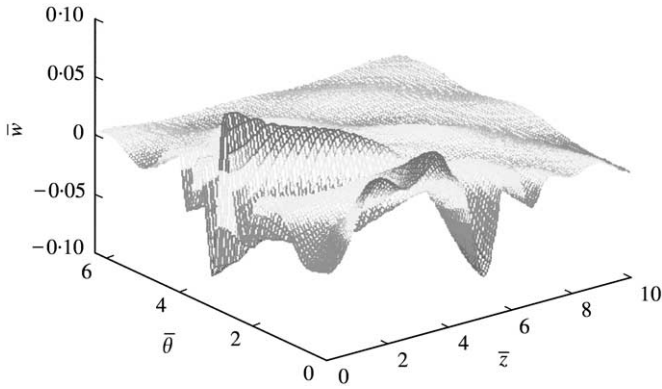


Figure 4. The response distribution of the radial displacement w on the outer surface of Type 1 shell ($R_1 = H$) subjected to a radial point load at ($z = 0, \theta = 0$) with a time history of one-cycle sine function.

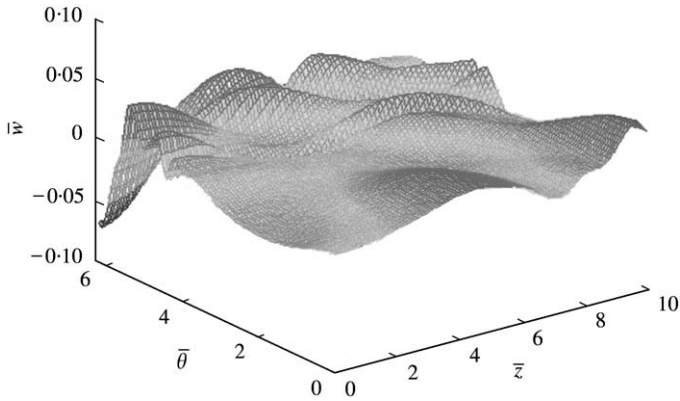


Figure 5. Same as Figure 3 but for Type 2 shell.

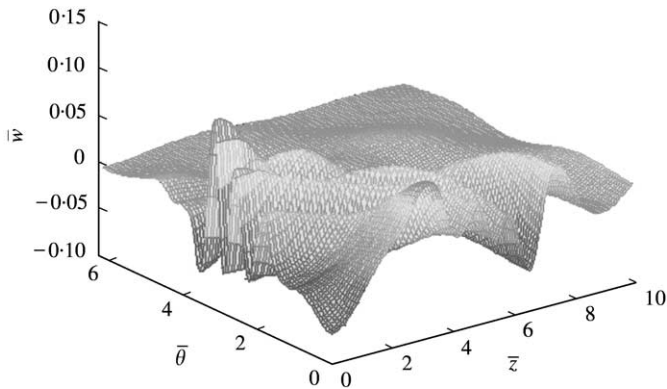


Figure 6. Same as Figure 3 but for Type 3 shell.

exponent n is presented. It is observed from Figure 8 that the peak value of displacement response of Type 1 increases as the power-law exponent n increases. This can be explained like this. Type 1 has silicon nitride material properties on the inner surface and stainless-steel material properties on the outer surface. Small values of n correspond to

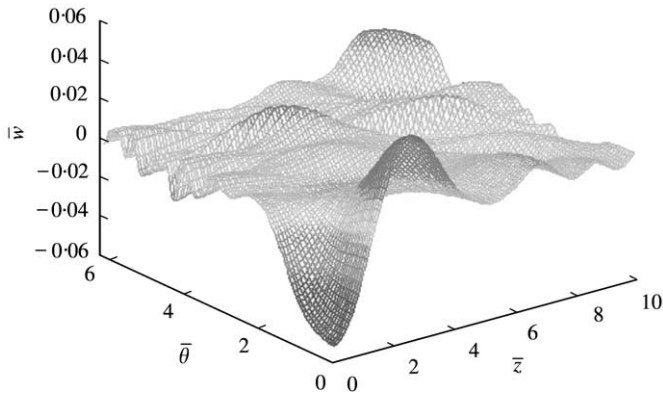


Figure 7. Same as Figure 3 but for Type 4 shell.

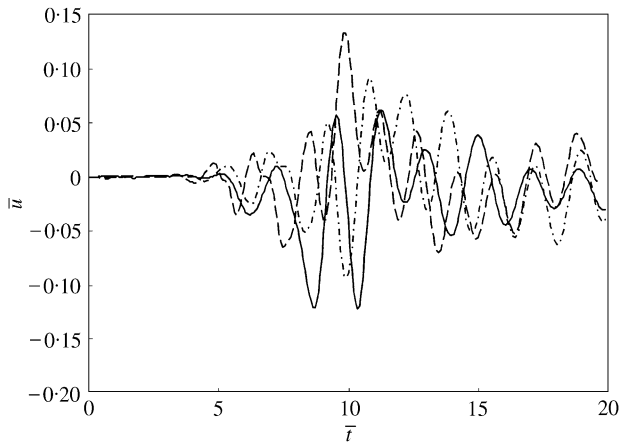


Figure 8. Time history of the displacement at $(z = 10.0, \theta = 0)$ on the outer surface of Type 1 shell ($R_1 = H$) excited by an incident wave at $(z = 0.0, \theta = 0)$. —, $n = 1.0$; - - - - -, $n = 2.0$; - · - · - ·, $n = 4.0$.

a large volume fraction of stainless steel whereas large values of n correspond to a large volume fraction of silicon nitride as shown in equation (45).

5.2. CHARACTERIZATION OF $z-t$ PLANE FOR THE FGM SHELL

To show the characteristics of waves, the so-called $x-t$ plane [19] is often used. Due to the inhomogeneity of the FGM, and the presence of boundaries, all kinds of waves are dispersive vector waves, and coupled to each other. Therefore, there is no pure longitudinal (P wave), or shear wave (S wave). Also, it is impossible to observe clear wave fronts of these waves in the $x-t$ plane. However, waves having similar properties of P and S waves can still be observed in the $x-t$ plane. These waves are called pseudo-P, and pseudo-S waves in this section, and are discussed in the following paragraphs.

Figures 9 and 10 show the $z-t$ plane for the displacement response u and w on the outer surface of Type 1 thin cylindrical shell subjected to a radial line load with a time history of one cycle of sine function at $z = 0$ respectively. From these two figures, it can be seen that at different times, different forms of wave fields are observed. The form of the wave field changes while waves propagate, because the waves are scattered by the boundaries and inhomogeneity of the shell. From Figure 9 the wave front of the pseudo-P wave can be quite

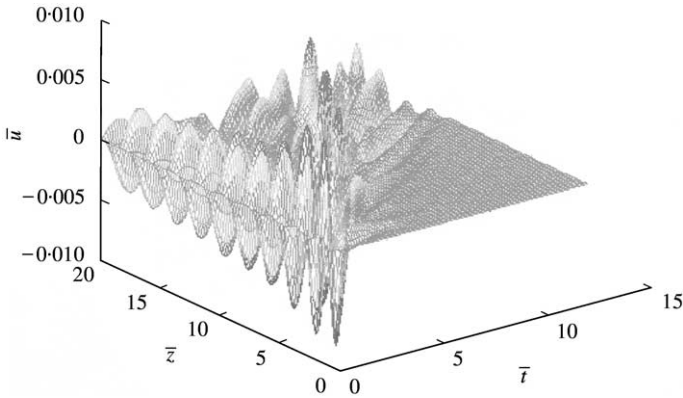


Figure 9. Displacement u on the outer surface in the $z-t$ plane of Type 1 cylindrical shell ($R_1/H = 20$).

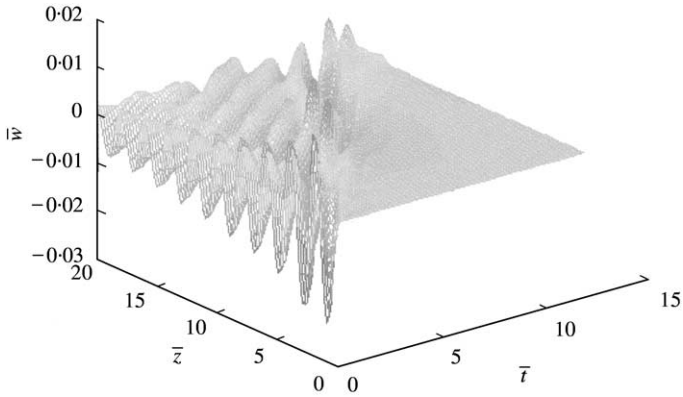


Figure 10. Same as Figure 9 but for displacement w .

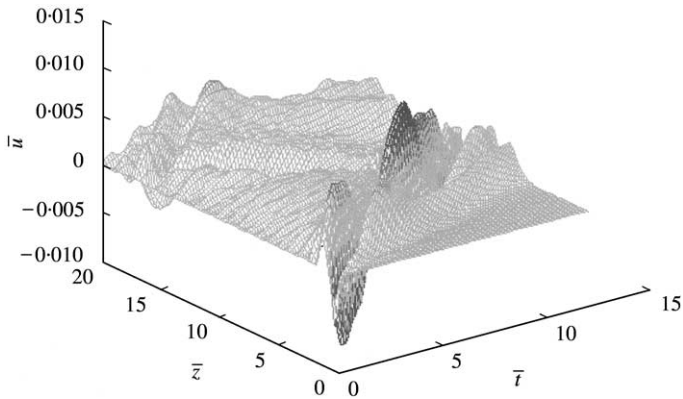


Figure 11. Displacement u on the outer surface in the $z-t$ plane of Type 2 cylindrical shell ($R_1/H = 20$).

clearly observed, as the displacement response u is sensitive to the pseudo-P wave. The wave front for the pseudo-P wave is less obvious in Figure 10, due to the fact that the displacement response w is less sensitive than the displacement response u . The wave front for the pseudo-S wave is quite obvious.

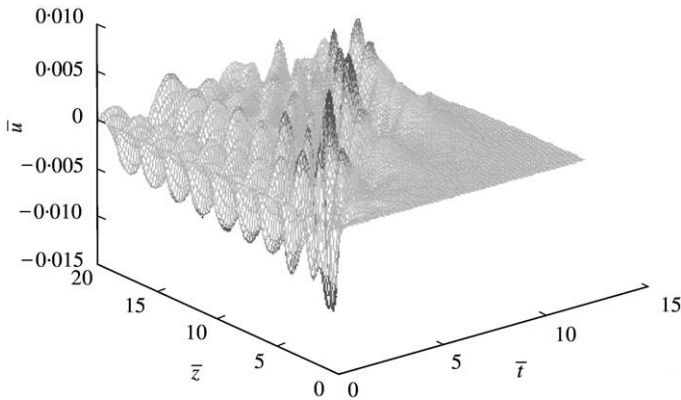


Figure 12. Displacement u on the outer surface in the z - t plane of Type 3 cylindrical shell ($R_1/H = 20$).

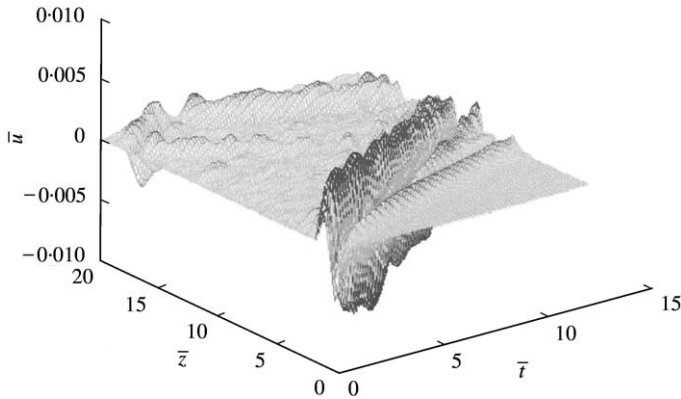


Figure 13. Displacement u on the outer surface in the z - t plane of Type 4 cylindrical shell ($R_1/H = 20$).

Figures 11, 12 and 13 illustrate the z - t plane for the displacement response u on the outer surface of Types 2, 3 and 4 cylindrical shells subjected to a radial line load with a time history of one cycle of sine function at $z = 0$ respectively. From these figures, we can obtain clear characteristics of waves in FGM cylindrical shells.

Furthermore, Figure 14 shows the time history of the displacement u on the outer surface of the shell subjected to a line load with a time history of one cycle of sine function at $z = 0$. A comparison of the displacement response between pure stainless-steel shell and Type 1 FGM shell ($n = 1$) is presented. It can be observed from Figure 14 that the peak value of displacement response for Type 1 FGM shell is less than that for the steel isotropic shell. The letters P and S in Figure 14 mark the arrival times of the dilatational and shear wave of the isotropic stainless steel.

As the transient wave response is considered in this study, the shell is treated as infinite in the co-ordinates z and θ . The boundary conditions, therefore, should be radiation conditions. In the present formulation of the wave propagation, these radiation conditions are satisfied naturally. Further study of the movement of wave front should be revealed in a transient response analysis; Li *et al.* [20] gave an exact solution for the transient response in a homogeneous cylindrical shell of finite length.

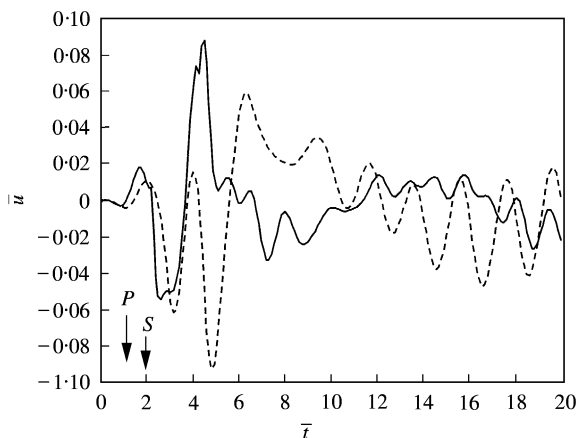


Figure 14. Comparison of time history of displacement u on the outer surface at $z = 2H$ subjected to a vertical line load with a time history of one cycle of sine function at $x = 0$ (—, stainless steel shell; ---, Type 1 shell ($n = 1$)).

6. CONCLUSION

A numerical method is presented to calculate the displacement response of FGM shells excited by impact loads. This method is straightforward to use for the analysis of arbitrary FGM shells subjected to point loads. The method takes into account the special property of FGM wherein the material properties change continuously in the thickness direction. The present method can be directly used for anisotropic laminated shells without any difficulty, by setting Δc_{ij}^n and $\Delta \rho_n$ equal to zero in equations (8) and (9). The use of layer elements through the radial direction makes it easier to deal with composite shells made of an arbitrary number of anisotropic layers, arbitrary lay-ups and any type of materials. Furthermore, the method is capable of reducing the spatial dimensions of a problem by one. It avoids tedious pre-processors that occupy a substantial part in finite element methods, consequently, it reduces a great deal of computational labor.

The examples have shown the applicability of the present method. For two-dimensional problems, the response calculation is very fast. The high efficiency paves the way for inverse procedures of material characterization of FGM shells, as there would be thousands of times of calling the forward calculation in an inverse operator.

REFERENCES

1. MIRSKY 1964 *Journal of the Acoustical Society of America* **36**, 2106–2112. Axisymmetric vibrations of orthotropic shells.
2. J. L. NOWINSKI 1967 *Journal of Engineering for Industry* **89**, 408–412. Propagation of longitudinal waves in circular cylindrical orthotropic bars.
3. F. H. CHOU and J. D. ACHENBACH 1981 *American Society of Civil Engineers Journal of Engineering Mechanics* **98**, 813–822. Three-dimensional vibrations of orthotropic cylinders.
4. K. H. HUANG and S. B. DONG 1984 *Journal of Sound and Vibration* **96**, 363–379. Propagating waves and edge vibration in anisotropic composite cylinders.
5. R. B. NELSON, S. B. DONG and R. D. KALRA 1971 *Journal of Sound and Vibration* **18**, 429–444. Vibrations and waves in laminated orthotropic circular cylinders.
6. F. G. YUAN and C. C. HSIEH 1998 *Composite Structures* **42**, 153–167. Three-dimensional wave propagation in composite cylindrical shells.
7. A. H. NAYFEH 1995 *Wave Propagation in Layered Anisotropic Media with Applications to Composites*. Amsterdam: Elsevier, North-Holland.

8. N. RATTANWANGCHAROEN, A. SHAH and S. K. DATTA 1994 *American Society of Mechanical Engineers Journal of Applied Mechanics* **61**, 323–329. Reflection of waves at the free edge of a laminated circular cylinder.
9. S. MARKUS and D. J. MEAD 1995 *Journal of Sound and Vibration* **181**, 127–147. Axisymmetric and asymmetric wave motion in orthotropic cylinders.
10. S. MARKUS and D. J. MEAD. 1995 *Journal of Sound and Vibration* **181**, 149–167. Wave motion in a 3-layered, orthotropic isotropic orthotropic composite shell.
11. Z. C. XI, G. R. LIU, K. Y. LAM and H. M. SHANG 1999 *American Society of Mechanical Engineers Journal of Applied Mechanics* **67**, 427–429. Strip element method for analyzing wave scattering by a crack in a laminated composite cylinder.
12. X. HAN, G. R. LIU, Z. C. XI and K. Y. LAM 2000. *International Journal of Solids and Structures* **38**, 3021–3037. Transient waves in a functionally graded cylinder.
13. J. R. VINSON and R. L. SIERAKOWSKI 1987 *The Behavior of Structures Composed of Composite Materials*. Dordrecht: Martinus Nijhoff.
14. G. R. LIU, J. TANI, T. OHYOSHI and K. WATANABE 1991 *Journal of Vibration and Acoustics* **113**, 230–239. Transient waves in anisotropic laminated plates. Part 1: theory; Part 2: applications.
15. G. R. LIU, K. Y. LAM and T. OHYOSHI 1997 *Composites Part B* **28**, 667–677. A technique for analyzing elastodynamic responses of anisotropic laminated plates to line loads.
16. A. D. PIERCE and H. G. KIL 1990 *Journal of Vibration and Acoustics* **112**, 399–406. Elastic wave propagation from point excitations on thin-walled cylindrical shells.
17. G. R. LIU, X. HAN and K. Y. LAM 2001 *Journal of Composite Materials* **35**, 954–971. Material Characterization of FGM plates using elastic waves and an inverse procedure.
18. Y. S. TOULOUKIAN 1967 *Thermophysical Properties of High Temperature Solid Materials*. New York: Macmillan.
19. K. F. GRAFF 1991 *Wave Motion in Elastic Solids*. New York: Dover Publications.
20. S. M. LI, H. Z. HONG and C. RUIZ, 1994 *International Journal of Solids and Structures* **27**, 485–503. Transient response of a cylindrical shell of finite length to transverse impact.

APPENDIX A

$$\mathbf{A}_1 = \frac{h_n}{60} \begin{bmatrix} (8r_n + h_n)\mathbf{D}_{11} & 4r_n \mathbf{D}_{11} & -(2r_n + h_n)\mathbf{D}_{11} \\ & (32r_n + 16h_n)\mathbf{D}_{11} & (4r_n + h_n)\mathbf{D}_{11} \\ \text{sym} & & (8r_n + 7h_n)\mathbf{D}_{11} \end{bmatrix},$$

where

$$\mathbf{D}_{11} = \mathbf{L}_1^T \mathbf{c}^I \mathbf{L}_1 = \begin{bmatrix} c_{11} & c_{16} & c_{15} \\ c_{16} & c_{66} & c_{56} \\ c_{51} & c_{56} & c_{55} \end{bmatrix}^I,$$

$$\mathbf{A}_2 = \frac{h_n}{30} \begin{bmatrix} 4(\mathbf{D}_{12} + \mathbf{D}_{12}^T) & 2(\mathbf{D}_{12} + \mathbf{D}_{12}^T) & -(\mathbf{D}_{12} + \mathbf{D}_{12}^T) \\ & 4(\mathbf{D}_{12} + \mathbf{D}_{12}^T) & 2(\mathbf{D}_{12} + \mathbf{D}_{12}^T) \\ \text{sym} & & 4(\mathbf{D}_{12} + \mathbf{D}_{12}^T) \end{bmatrix},$$

where

$$\mathbf{D}_{12} = \mathbf{L}_1^T \mathbf{c}^I \mathbf{L}_2 = \begin{bmatrix} c_{16} & c_{12} & c_{14} \\ c_{66} & c_{26} & c_{46} \\ c_{56} & c_{52} & c_{45} \end{bmatrix}^I,$$

$$\mathbf{A}_3 = \frac{1}{6h_n^4} \begin{bmatrix} \alpha_{11} \mathbf{D}_{33} & \alpha_{12} \mathbf{D}_{33} & \alpha_{13} \mathbf{D}_{33} \\ \alpha_{12} \mathbf{D}_{33} & \alpha_{22} \mathbf{D}_{33} & \alpha_{23} \mathbf{D}_{33} \\ \alpha_{13} \mathbf{D}_{33} & \alpha_{23} \mathbf{D}_{33} & \alpha_{33} \mathbf{D}_{33} \end{bmatrix},$$

where

$$\begin{aligned} \alpha_{11} = & -24h_n r_n^3 - 15h_n^4 - 60h_n^2 r_n^2 - 50h_n^3 r_n + 6 \ln(r_n + h_n) h_n^4 + 36 \ln(r_n + h_n) r_n h_n^3 \\ & + 78 \ln(r_n + h_n) R_n^2 h_n^2 + 72 \ln(r_n + h_n) R_n^3 h_n + 24 \ln(r_n + h_n) r_n^4 - 6 \ln(r_n) h_n^4 \\ & - 36 \ln(r_n) r_n h_n^3 - 78 \ln(r_n) r_n^2 h_n^2 - 72 \ln(r_n) r_n^3 h_n - 24 \ln(r_n) r_n^4, \end{aligned}$$

$$\begin{aligned} \alpha_{12} = & -4[-12h_n r_n^3 - h_n^4 - 24h_n^2 r_n^2 - 13h_n^3 r_n + 6 \ln(r_n + h_n) r_n h_n^3 + 24 \ln(r_n + h_n) r_n^2 h_n^2 \\ & + 30 \ln(r_n + h_n) r_n^3 h_n + 12 \ln(r_n + h_n) r_n^4 - 6 \ln(r_n) r_n h_n^3 - 24 \ln(r_n) r_n^2 h_n^2 \\ & - 30 \ln(r_n) r_n^3 h_n - 12 \ln(r_n) r_n^4], \end{aligned}$$

$$\begin{aligned} \alpha_{13} = & -24h_n r_n^3 - h_n^4 - 36h_n^2 r_n^2 - 14h_n^3 r_n + 6 \ln(r_n + h_n) r_n h_n^3 + 30 \ln(r_n + h_n) r_n^2 h_n^2 \\ & + 48 \ln(r_n + h_n) r_n^3 h_n + 24 \ln(r_n + h_n) r_n^4 - 6 \ln(r_n) r_n h_n^3 - 30 \ln(r_n) r_n^2 h_n^2 \\ & - 48 \ln(r_n) r_n^3 h_n - 24 \ln(r_n) r_n^4, \end{aligned}$$

$$\begin{aligned} \alpha_{22} = & 8[-12h_n r_n^3 + h_n^4 - 18h_n^2 r_n^2 + 12 \ln(r_n + h_n) r_n^2 h_n^2 - 4h_n^3 r_n + 24 \ln(r_n + h_n) r_n^3 h_n \\ & + 12 \ln(r_n + h_n) r_n^4 - 12 \ln(r_n) r_n^2 h_n^2 - 24 \ln(r_n) r_n^3 h_n - 12 \ln(r_n) r_n^4], \end{aligned}$$

$$\begin{aligned} \alpha_{23} = & -4[-12h_n r_n^2 - 12h_n^2 r_n + 6 \ln(r_n + h_n) r_n h_n^2 - h_n^3 + 18 \ln(r_n + h_n) r_n^2 h_n \\ & + 12 \ln(r_n + h_n) r_n^3 - 6 \ln(r_n) r_n h_n^2 - 18 \ln(r_n) r_n^2 h_n - 12 \ln(r_n) r_n^3], \end{aligned}$$

$$\begin{aligned} \alpha_{33} = & -24h_n r_n^3 + h_n^4 - 12h_n^2 r_n^2 + 6 \ln(r_n + h_n) r_n^2 h_n^2 - 2h_n^3 r_n + 24 \ln(r_n + h_n) r_n^3 h_n \\ & + 24 \ln(r_n + h_n) r_n^4 - 6 \ln(r_n) r_n^2 h_n^2 - 24 \ln(r_n) r_n^3 h_n - 24 \ln(r_n) r_n^4, \end{aligned}$$

$$\mathbf{D}_{33} = \mathbf{L}_3^T \mathbf{c}^I \mathbf{L}_3 = \begin{bmatrix} c_{55} & c_{45} & c_{53} \\ c_{45} & c_{44} & c_{43} \\ c_{35} & c_{34} & c_{33} \end{bmatrix}^I,$$

$$\begin{aligned} \mathbf{A}_4 = & \frac{1}{30} \begin{bmatrix} (-15r_n - 2h_n)\mathbf{D}_{13}^T & (-20r_n - 6h_n)\mathbf{D}_{13}^T & (5r_n + 3h_n)\mathbf{D}_{13}^T \\ (20r_n + 4h_n)\mathbf{D}_{13}^T & -8h_n\mathbf{D}_{13}^T & (-20r_n - 16h_n)\mathbf{D}_{13}^T \\ (-5r_n - 2h_n)\mathbf{D}_{13}^T & (20r_n + 14h_n)\mathbf{D}_{13}^T & (15r_n + 3h_n)\mathbf{D}_{13}^T \end{bmatrix} \\ & + \frac{h_n}{30} \begin{bmatrix} 4\mathbf{D}_{14}^T & 2\mathbf{D}_{14}^T & -\mathbf{D}_{14}^T \\ & 4\mathbf{D}_{14}^T & 2\mathbf{D}_{14}^T \\ \text{sym} & & 4\mathbf{D}_{14}^T \end{bmatrix} - \frac{h_n}{30} \begin{bmatrix} 4\mathbf{D}_{14} & 2\mathbf{D}_{14} & -\mathbf{D}_{14} \\ & 4\mathbf{D}_{14} & 2\mathbf{D}_{14} \\ \text{sym} & & 4\mathbf{D}_{14} \end{bmatrix} \\ & - \frac{1}{30} \begin{bmatrix} (-15r_n - 2h_n)\mathbf{D}_{13} & (20r_n + 4h_n)\mathbf{D}_{13} & (-5r_n - 2h_n)\mathbf{D}_{13} \\ (-20r_n - 5h_n)\mathbf{D}_{13} & -8h_n\mathbf{D}_{13} & (20r_n + 14h_n)\mathbf{D}_{13} \\ (5r_n + 3h_n)\mathbf{D}_{13} & (-20r_n - 16h_n)\mathbf{D}_{13} & (15r_n + 13h_n)\mathbf{D}_{13} \end{bmatrix}, \end{aligned}$$

where

$$\mathbf{D}_{13} = \mathbf{L}_1^T \mathbf{c}^I \mathbf{L}_3 = \begin{bmatrix} c_{15} & c_{13} & c_{13} \\ c_{56} & c_{46} & c_{36} \\ c_{55} & c_{45} & c_{53} \end{bmatrix}^I, \quad \mathbf{D}_{14} = \mathbf{L}_1^T \mathbf{c}^I \mathbf{L}_4 = \begin{bmatrix} 0 & -c_{14} & c_{12} \\ 0 & -c_{46} & c_{26} \\ 0 & -c_{45} & c_{52} \end{bmatrix}^I,$$

$$\begin{aligned} \mathbf{A}_5 = & \frac{1}{6h_n^4} \begin{bmatrix} \alpha_{11}(\mathbf{D}_{24}^T - \mathbf{D}_{24}) & \alpha_{12}(\mathbf{D}_{24}^T - \mathbf{D}_{24}) & \alpha_{13}(\mathbf{D}_{24}^T - \mathbf{D}_{24}) \\ \alpha_{12}(\mathbf{D}_{24}^T - \mathbf{D}_{24}) & \alpha_{22}(\mathbf{D}_{24}^T - \mathbf{D}_{24}) & \alpha_{23}(\mathbf{D}_{24}^T - \mathbf{D}_{24}) \\ \alpha_{13}(\mathbf{D}_{24}^T - \mathbf{D}_{24}) & \alpha_{23}(\mathbf{D}_{24}^T - \mathbf{D}_{24}) & \alpha_{33}(\mathbf{D}_{24}^T - \mathbf{D}_{24}) \end{bmatrix} \\ & + \frac{1}{6} \begin{bmatrix} -3\mathbf{D}_{23}^T & -4\mathbf{D}_{23}^T & \mathbf{D}_{23}^T \\ 4\mathbf{D}_{23}^T & 0 & -4\mathbf{D}_{23}^T \\ -\mathbf{D}_{23}^T & 4\mathbf{D}_{23}^T & 3\mathbf{D}_{23}^T \end{bmatrix} - \frac{1}{6} \begin{bmatrix} -3\mathbf{D}_{23} & 4\mathbf{D}_{23} & -\mathbf{D}_{23} \\ -4\mathbf{D}_{23} & 0 & 4\mathbf{D}_{23} \\ \mathbf{D}_{23} & -4\mathbf{D}_{23} & 3\mathbf{D}_{23} \end{bmatrix} \end{aligned}$$

where

$$\mathbf{D}_{24} = \mathbf{L}_2^T \mathbf{c}^I \mathbf{L}_4 = \begin{bmatrix} 0 & -c_{46} & c_{26} \\ 0 & -c_{24} & c_{22} \\ 0 & -c_{44} & c_{42} \end{bmatrix}^I, \quad \mathbf{D}_{23} = \mathbf{L}_2^T \mathbf{c}^I \mathbf{L}_3 = \begin{bmatrix} c_{56} & c_{46} & c_{36} \\ c_{25} & c_{24} & c_{23} \\ c_{45} & c_{44} & c_{43} \end{bmatrix}^I,$$

$$\begin{aligned} \mathbf{A}_6 = & \frac{1}{6h_n^4} \begin{bmatrix} \alpha_{11}\mathbf{D}_{44} & \alpha_{12}\mathbf{D}_{44} & \alpha_{13}\mathbf{D}_{44} \\ \alpha_{12}\mathbf{D}_{44} & \alpha_{22}\mathbf{D}_{44} & \alpha_{23}\mathbf{D}_{44} \\ \alpha_{13}\mathbf{D}_{44} & \alpha_{23}\mathbf{D}_{44} & \alpha_{33}\mathbf{D}_{44} \end{bmatrix} \\ & + \frac{1}{6} \begin{bmatrix} -3\mathbf{D}_{34}^T & 4\mathbf{D}_{34}^T & -\mathbf{D}_{34}^T \\ -4\mathbf{D}_{34}^T & 0 & 4\mathbf{D}_{34}^T \\ \mathbf{D}_{34}^T & -4\mathbf{D}_{34}^T & 3\mathbf{D}_{34}^T \end{bmatrix} + \frac{1}{6} \begin{bmatrix} -3\mathbf{D}_{34} & -4\mathbf{D}_{34} & \mathbf{D}_{34} \\ 4\mathbf{D}_{34} & 0 & -4\mathbf{D}_{34} \\ -\mathbf{D}_{34} & 4\mathbf{D}_{34} & 3\mathbf{D}_{34} \end{bmatrix} \end{aligned}$$

$$+ \frac{1}{6h_n} \begin{bmatrix} (14r_n + 3h_n)\mathbf{D}_{33} & (-16r_n - 4h_n)\mathbf{D}_{33} & (2r_n + h_n)\mathbf{D}_{33} \\ & (32r_n + 16h_n)\mathbf{D}_{33} & (-16r_n - 12h_n)\mathbf{D}_{33} \\ \text{sym} & & (14r_n + 11h_n)\mathbf{D}_{33} \end{bmatrix},$$

where

$$\mathbf{D}_{44} = \mathbf{L}_4^T \mathbf{c}^I \mathbf{L}_4 = \begin{bmatrix} 0 & 0 & 0 \\ 0 & c_{44} & -c_{42} \\ 0 & c_{24} & c_{22} \end{bmatrix}^I, \quad \mathbf{D}_{34} = \mathbf{L}_3^T \mathbf{c}^I \mathbf{L}_4 = \begin{bmatrix} 0 & -c_{45} & c_{52} \\ 0 & -c_{44} & c_{42} \\ 0 & -c_{34} & c_{23} \end{bmatrix}^I,$$

$$\mathbf{D}_{33} = \mathbf{L}_3^T \mathbf{c}^I \mathbf{L}_3 = \begin{bmatrix} c_{55} & c_{52} & c_{45} \\ c_{46} & c_{42} & c_{44} \\ c_{36} & c_{23} & c_{34} \end{bmatrix}^I,$$

$$\mathbf{M} = \frac{\rho^I h_n}{60} \begin{bmatrix} (8r_n + h_n)\mathbf{E} & 4r_n\mathbf{E} & -(2r_n + h_n)\mathbf{E} \\ 4r_n\mathbf{E} & (32r_n + 16h_n)\mathbf{E} & (4r_n + 4h_n)\mathbf{E} \\ -(2r_n + h_n)\mathbf{E} & (4r_n + 4h_n)\mathbf{E} & (8r_n + 7h_n)\mathbf{E} \end{bmatrix}.$$

APPENDIX B

$$\mathbf{A}_1^d = \frac{h_n}{420} \begin{bmatrix} (7h_n r_n + 2h_n^2)\Delta\mathbf{D}_{11} & -4h_n^2\mathbf{D}_{11} & -(7h_n r_n + 5h_n^2)\Delta\mathbf{D}_{11} \\ & (112r_n h_n + 64h_n^2)\Delta\mathbf{D}_{11} & (28r_n h_n + 24h_n^2)\Delta\mathbf{D}_{11} \\ \text{sym} & & (49h_n r_n + 44h_n^2)\Delta\mathbf{D}_{11} \end{bmatrix},$$

where

$$\Delta\mathbf{D}_{11} = \frac{1}{h_n} \mathbf{L}_1^T (\mathbf{c}^O - \mathbf{c}^I) \mathbf{L}_1 = \frac{1}{h_n} \begin{bmatrix} \Delta c_{11} & \Delta c_{16} & \Delta c_{15} \\ \Delta c_{16} & \Delta c_{66} & \Delta c_{56} \\ \Delta c_{51} & \Delta c_{56} & \Delta c_{55} \end{bmatrix}_n,$$

$$\mathbf{A}_2^d = \frac{h_n^2}{60} \begin{bmatrix} (\Delta\mathbf{D}_{12} + \Delta\mathbf{D}_{12}^T) & 0 & -(\Delta\mathbf{D}_{12} + \Delta\mathbf{D}_{12}^T) \\ & 16(\Delta\mathbf{D}_{12} + \Delta\mathbf{D}_{12}^T) & 4(\Delta\mathbf{D}_{12} + \Delta\mathbf{D}_{12}^T) \\ \text{sym} & & 7(\Delta\mathbf{D}_{12} + \Delta\mathbf{D}_{12}^T) \end{bmatrix},$$

where

$$\Delta\mathbf{D}_{12} = \frac{1}{h_n} \mathbf{L}_1^T (\mathbf{c}^O - \mathbf{c}^I) \mathbf{L}_2 = \frac{1}{h_n} \begin{bmatrix} \Delta c_{16} & \Delta c_{12} & \Delta c_{14} \\ \Delta c_{66} & \Delta c_{26} & \Delta c_{46} \\ \Delta c_{56} & \Delta c_{52} & \Delta c_{45} \end{bmatrix}_n,$$

$$\mathbf{A}_3^d = \frac{1}{60h_n^4} \begin{bmatrix} \alpha'_{11}\Delta\mathbf{D}_{33} & \alpha'_{12}\Delta\mathbf{D}_{33} & \alpha'_{13}\Delta\mathbf{D}_{33} \\ \alpha'_{12}\Delta\mathbf{D}_{33} & \alpha'_{22}\Delta\mathbf{D}_{33} & \alpha'_{23}\Delta\mathbf{D}_{33} \\ \alpha'_{13}\Delta\mathbf{D}_{33} & \alpha'_{23}\Delta\mathbf{D}_{33} & \alpha'_{33}\Delta\mathbf{D}_{33} \end{bmatrix},$$

where

$$\begin{aligned} \alpha'_{11} = & 2[4h_n^5 + 75h_n^4r_n + 250r_n^2h_n^3 + 300r_n^3h_n^2 + 120r_n^4h_n - 30r \ln(r_n + h_n)h_n^4 \\ & - 180r_n^2 \ln(h_n + r_n)h_n^3 - 390r_n^3 \ln(h_n + r_n)h_n^2 - 360r_n^4 \ln(h_n + r_n)h_n - 120r_n^5 \ln(r_n + h_n) \\ & + 180r_n^2 \ln(r_n)h_n^3 + 30r_n \ln(r_n)h_n^4 + 360r_n^4 \ln(r_n)h_n + 390r_n^3 \ln(r_n)h_n^2 + 120r_n^5 \ln(r_n)], \end{aligned}$$

$$\begin{aligned} \alpha'_{12} = & 4[h_n^5 - 10h_n^4r_n - 130r_n^2h_n^3 - 240r_n^3h_n^2 - 120r_n^4r_n \\ & + 60r_n^2 \ln(h_n + r_n)h_n^3 + 240r_n^3 \ln(h_n + r_n)h_n^2 + 300r_n^4 \ln(h_n + r_n)h_n + 120r_n^5 \ln(r_n + h_n) \\ & - 60r_n^2 \ln(r_n)h_n^3 - 300r_n^4 \ln(r_n)h_n - 240r_n^3 \ln(r_n)h_n^2 - 120r_n^5 \ln(r_n)], \end{aligned}$$

$$\begin{aligned} \alpha'_{13} = & -2[h_n^5 - 5h_n^4r_n - 70r_n^2h_n^3 - 180r_n^3h_n^2 - 120r_n^4h_n + 30r_n^2 \ln(h_n + r_n)h_n^3 \\ & + 150r_n^3 \ln(h_n + r_n)h_n^2 + 240r_n^4 \ln(h_n + r_n)h_n + 120r_n^5 \ln(r_n + h_n) \\ & - 30r_n^2 \ln(r_n)h_n^3 - 240r_n^4 \ln(r_n)h_n - 150r_n^3 \ln(r_n)h_n^2 - 120r_n^5 \ln(r_n)], \end{aligned}$$

$$\begin{aligned} \alpha'_{22} = & 16[2h_n^5 - 5h_n^4r_n + 20r_n^2h_n^3 + 90r_n^3h_n^2 + 60r_n^4h_n \\ & - 60r_n^3 \ln(h_n + r_n)h_n^2 - 120r_n^4 \ln(h_n + r_n)h_n - 60r_n^5 \ln(r_n + h_n) \\ & + 120r_n^4 \ln(r_n)h_n + 60r_n^3 \ln(r_n)h_n^2 + 60r_n^5 \ln(r_n)], \end{aligned}$$

$$\begin{aligned} \alpha'_{23} = & 4[h_n^5 - 120h_n^4r_n - 10r_n^2h_n^3 - 120r_n^3h_n^2 \\ & + 60r_n^3 \ln(h_n + r_n)h_n^2 + 180r_n^4 \ln(h_n + r_n)h_n + 120r_n^5 \ln(r_n + h_n) \\ & - 180r_n^4 \ln(r_n)h_n - 60r_n^3 \ln(r_n)h_n^2 - 120r_n^5 \ln(r_n)], \end{aligned}$$

$$\begin{aligned} \alpha'_{33} = & 2[4h_n^5 - 5h_n^4r_n + 10r_n^2h_n^3 + 60r_n^3h_n^2 + 120r_n^4h_n \\ & - 30r_n^3 \ln(h_n + r_n)h_n - 120r_n^4 \ln(h_n + r_n)h_n - 120r_n^5 \ln(r_n + h_n) \\ & + 120r_n^4 \ln(r_n)h_n + 30r_n^3 \ln(r_n)h_n^2 + 120r_n^5 \ln(r_n)], \end{aligned}$$

$$\Delta \mathbf{D}_{33} = \frac{1}{h_n} \mathbf{L}_3^T (\mathbf{c}^O - \mathbf{c}^I) \mathbf{L}_3 = \frac{1}{h_n} \begin{bmatrix} \Delta c_{55} & \Delta c_{45} & \Delta c_{53} \\ \Delta c_{45} & \Delta c_{44} & \Delta c_{43} \\ \Delta c_{35} & \Delta c_{34} & \Delta c_{33} \end{bmatrix}^T,$$

$$\begin{aligned} \mathbf{A}_4^d = & \frac{h_n}{60} \begin{bmatrix} (-4r_n - h_n) \Delta \mathbf{D}_{13}^T & (-12r_n - 4h_n) \Delta \mathbf{D}_{13}^T & (6r_n + 5h_n) \Delta \mathbf{D}_{13}^T \\ (8r_n + 4h_n) \Delta \mathbf{D}_{13}^T & -16(h_n + r_n) \Delta \mathbf{D}_{13}^T & (-32r_n - 28h_n) \Delta \mathbf{D}_{13}^T \\ (-4r_n - 3h_n) \Delta \mathbf{D}_{13}^T & (28r_n + 20h_n) \Delta \mathbf{D}_{13}^T & (26r_n + 23h_n) \Delta \mathbf{D}_{13}^T \end{bmatrix} \\ & + \frac{h_n^2}{60} \begin{bmatrix} \Delta \mathbf{D}_{14}^T & 0 & -\Delta \mathbf{D}_{14}^T \\ & 16 \Delta \mathbf{D}_{14}^T & 4 \Delta \mathbf{D}_{14}^T \\ \text{sym} & & 7 \Delta \mathbf{D}_{14}^T \end{bmatrix} - \frac{h_n^2}{60} \begin{bmatrix} \Delta \mathbf{D}_{14} & 0 & -\Delta \mathbf{D}_{14} \\ & 16 \Delta \mathbf{D}_{14} & 4 \Delta \mathbf{D}_{14} \\ \text{sym} & & 7 \Delta \mathbf{D}_{14} \end{bmatrix} \end{aligned}$$

$$-\frac{h_n^2}{60} \begin{bmatrix} (-4r_n - h_n)\Delta\mathbf{D}_{13} & (8r_n + 4h_n)\Delta\mathbf{D}_{13} & (-4r_n - 3h_n)\Delta\mathbf{D}_{13} \\ (-12r_n - 4h_n)\Delta\mathbf{D}_{13} & -16(h_n + r_n)\Delta\mathbf{D}_{13} & (28r_n + 20h_n)\Delta\mathbf{D}_{13} \\ (6r_n + 5h_n)\Delta\mathbf{D}_{13} & (-32r_n - 28h_n)\Delta\mathbf{D}_{13} & (26r_n + 23h_n)\Delta\mathbf{D}_{13} \end{bmatrix},$$

where

$$\Delta\mathbf{D}_{13} = \frac{1}{h_n} \mathbf{L}_1^T (\mathbf{c}^O - \mathbf{c}^I) \mathbf{L}_3 = \frac{1}{h_n} \begin{bmatrix} \Delta c_{15} & \Delta c_{14} & \Delta c_{13} \\ \Delta c_{56} & \Delta c_{46} & \Delta c_{36} \\ \Delta c_{55} & \Delta c_{45} & \Delta c_{53} \end{bmatrix}_n,$$

$$\Delta\mathbf{D}_{14} = \frac{1}{h_n} \mathbf{L}_1^T (\mathbf{c}^O - \mathbf{c}^I) \mathbf{L}_4 = \frac{1}{h_n} \begin{bmatrix} 0 & -\Delta c_{14} & \Delta c_{12} \\ 0 & -\Delta c_{46} & \Delta c_{26} \\ 0 & -\Delta c_{45} & \Delta c_{52} \end{bmatrix}_n,$$

$$\mathbf{A}_5^d = \frac{1}{60h_n^4} \begin{bmatrix} \alpha'_{11}(\Delta\mathbf{D}_{24}^T - \Delta\mathbf{D}_{24}) & \alpha'_{12}(\Delta\mathbf{D}_{24}^T - \Delta\mathbf{D}_{24}) & \alpha'_{13}(\Delta\mathbf{D}_{24}^T - \Delta\mathbf{D}_{24}) \\ \alpha'_{12}(\Delta\mathbf{D}_{24}^T - \Delta\mathbf{D}_{24}) & \alpha'_{22}(\Delta\mathbf{D}_{24}^T - \Delta\mathbf{D}_{24}) & \alpha'_{23}(\Delta\mathbf{D}_{24}^T - \Delta\mathbf{D}_{24}) \\ \alpha'_{13}(\Delta\mathbf{D}_{24}^T - \Delta\mathbf{D}_{24}) & \alpha'_{23}(\Delta\mathbf{D}_{24}^T - \Delta\mathbf{D}_{24}) & \alpha'_{33}(\Delta\mathbf{D}_{24}^T - \Delta\mathbf{D}_{24}) \end{bmatrix} \\ + \frac{h_n}{30} \begin{bmatrix} -2\Delta\mathbf{D}_{23}^T & -6\Delta\mathbf{D}_{23}^T & 3\Delta\mathbf{D}_{23}^T \\ 4\Delta\mathbf{D}_{23}^T & -8\Delta\mathbf{D}_{23}^T & -16\Delta\mathbf{D}_{23}^T \\ -2\Delta\mathbf{D}_{23}^T & 14\Delta\mathbf{D}_{23}^T & 13\Delta\mathbf{D}_{23}^T \end{bmatrix} - \frac{h_n}{30} \begin{bmatrix} -2\Delta\mathbf{D}_{23} & 4\Delta\mathbf{D}_{23} & -2\Delta\mathbf{D}_{23} \\ -6\Delta\mathbf{D}_{23} & -8\Delta\mathbf{D}_{23} & 14\Delta\mathbf{D}_{23} \\ 3\Delta\mathbf{D}_{23} & -16\Delta\mathbf{D}_{23} & 13\Delta\mathbf{D}_{23} \end{bmatrix},$$

$$\Delta\mathbf{D}_{24} = \frac{1}{h_n} \mathbf{L}_2^T (\mathbf{c}^O - \mathbf{c}^I) \mathbf{L}_4 = \frac{1}{h_n} \begin{bmatrix} 0 & -\Delta c_{46} & \Delta c_{26} \\ 0 & -\Delta c_{24} & \Delta c_{22} \\ 0 & -\Delta c_{44} & \Delta c_{42} \end{bmatrix}_n,$$

$$\Delta\mathbf{D}_{23} = \frac{1}{h_n} \mathbf{L}_2^T (\mathbf{c}^O - \mathbf{c}^I) \mathbf{L}_3 = \frac{1}{h_n} \begin{bmatrix} \Delta c_{56} & \Delta c_{46} & \Delta c_{36} \\ \Delta c_{25} & \Delta c_{24} & \Delta c_{23} \\ \Delta c_{45} & \Delta c_{44} & \Delta c_{43} \end{bmatrix}_n,$$

$$\mathbf{A}_6^d = \frac{1}{60h_n^4} \begin{bmatrix} \alpha'_{11}\Delta\mathbf{D}_{44} & \alpha'_{12}\Delta\mathbf{D}_{44} & \alpha'_{13}\Delta\mathbf{D}_{44} \\ \alpha'_{12}\Delta\mathbf{D}_{44} & \alpha'_{22}\Delta\mathbf{D}_{44} & \alpha'_{23}\Delta\mathbf{D}_{44} \\ \alpha'_{13}\Delta\mathbf{D}_{44} & \alpha'_{23}\Delta\mathbf{D}_{44} & \alpha'_{33}\Delta\mathbf{D}_{44} \end{bmatrix} \\ + \frac{h_n}{30} \begin{bmatrix} -2\Delta\mathbf{D}_{34}^T & -6\Delta\mathbf{D}_{34}^T & -3\Delta\mathbf{D}_{34}^T \\ 4\Delta\mathbf{D}_{34}^T & 8\Delta\mathbf{D}_{34}^T & -16\Delta\mathbf{D}_{34}^T \\ 2\Delta\mathbf{D}_{34}^T & 14\Delta\mathbf{D}_{34}^T & 13\Delta\mathbf{D}_{34}^T \end{bmatrix} + \frac{1}{6} \begin{bmatrix} -2\Delta\mathbf{D}_{34} & 4\Delta\mathbf{D}_{34} & 2\Delta\mathbf{D}_{34} \\ -6\Delta\mathbf{D}_{34} & -8\Delta\mathbf{D}_{34} & 14\Delta\mathbf{D}_{34} \\ -3\Delta\mathbf{D}_{34} & -16\Delta\mathbf{D}_{34} & 13\Delta\mathbf{D}_{34} \end{bmatrix} \\ + \frac{1}{30} \begin{bmatrix} (15r_n + 15h_n)\Delta\mathbf{D}_{33} & (-20r_n - 12h_n)\Delta\mathbf{D}_{33} & (5r_n + 6h_n)\Delta\mathbf{D}_{33} \\ & (80r_n + 64h_n)\Delta\mathbf{D}_{33} & (-15r_n - 52h_n)\Delta\mathbf{D}_{33} \\ & & (55r_n + 46h_n)\Delta\mathbf{D}_{33} \end{bmatrix},$$

sym

where

$$\Delta \mathbf{D}_{44} = \frac{1}{h_n} \mathbf{L}_4^T (\mathbf{c}^O - \mathbf{c}^I) \mathbf{L}_4 = \frac{1}{h_n} \begin{bmatrix} 0 & 0 & 0 \\ 0 & \Delta c_{44} & -\Delta c_{42} \\ 0 & \Delta c_{24} & \Delta c_{22} \end{bmatrix}_n,$$

$$\Delta \mathbf{D}_{34} = \frac{1}{h_n} \mathbf{L}_3^T (\mathbf{c}^O - \mathbf{c}^I) \mathbf{L}_4 = \frac{1}{h_n} \begin{bmatrix} 0 & -\Delta c_{45} & \Delta c_{52} \\ 0 & -\Delta c_{44} & \Delta c_{42} \\ 0 & -\Delta c_{34} & \Delta c_{23} \end{bmatrix}_n,$$

$$\Delta \mathbf{D}_{33} = \frac{1}{h_n} \mathbf{L}_3^T (\mathbf{c}^O - \mathbf{c}^I) \mathbf{L}_3 = \frac{1}{h_n} \begin{bmatrix} \Delta c_{55} & \Delta c_{52} & \Delta c_{45} \\ \Delta c_{46} & \Delta c_{42} & \Delta c_{44} \\ \Delta c_{36} & \Delta c_{23} & \Delta c_{34} \end{bmatrix}_n,$$

$$\mathbf{M}_d = \frac{h_n^2 \Delta \rho_n}{420} \begin{bmatrix} (2h_n + 7r_n)\mathbf{E} & -4h_n\mathbf{E} & -(5h_n + 7r_n)\mathbf{E} \\ & 16(4h_n + 7r_n)\mathbf{E} & 4(6h_n + 7r_n)\mathbf{E} \\ \text{sym} & & (44h_n + 49r_n)\mathbf{E} \end{bmatrix},$$

where

$$\Delta c_{ij} = (c_{ij}^O - c_{ij}^I)_n, \quad \Delta \rho_n = (\rho^O - \rho^I)_n.$$

APPENDIX C: NOMENCLATURE

\mathbf{c}	matrix of elastic constants
c	wave velocity
\mathbf{d}	displacement vector
$\tilde{\mathbf{d}}$	Fourier transformation of nodal displacement vector
\mathbf{E}	3×3 identity matrix
E	Young's modulus of elasticity
\mathbf{F}, \mathbf{T}	external force vector
$\tilde{\mathbf{F}}, \tilde{\mathbf{T}}$	Fourier transformation of external force vector
H	thickness of the structure
h_n	thickness of the n th layer element
$\mathbf{H}(t)$	Heaviside step function
$i = \sqrt{-1}$	imaginary unit
\mathbf{K}	stiffness matrix
\mathbf{L}	differential operator matrix
\mathbf{M}	mass matrix
\mathbf{N}	shape function matrix
R_1, R_2	inner radius and outer radius of the shell
t	time
\mathbf{U}	displacement vector
u, v, w	displacement components
V	volume fraction
r, θ, z	cylindrical co-ordinates
$\delta(x)$	the Dirac delta function
$\boldsymbol{\sigma}$	vector of stresses
$\boldsymbol{\varepsilon}$	vector of strains
$\boldsymbol{\psi}$	eigenvector

ω_m m th eigenfrequency
 ρ mass density
 ν the Poisson ratio

Superscripts

I, M, O inner, middle and outer surface of a layer element for shell respectively
T transposed matrix

Subscripts

$1, 2, \dots, n$ number of layer elements